Electronic Supplementary Material (ESI) for Physical Chemistry Chemical Physics
This journal is © The Owner Societies 2014

Supporting Information

Effect of Chromophore Encapsulation on Linear and Nonlinear Optical Properties: The Case of "miniSOG", a Protein-Encased Flavin

Nanna H. List,[†] Frederico M. Pimenta,[‡] Lotte Holmegaard,[‡] Rasmus L. Jensen,[‡] Michael Etzerodt,[¶] Tobias Schwabe,[§] Jacob Kongsted,[*,†] Peter R. Ogilby,[*,‡] and Ove Christiansen[*,‡]

Department of Physics, Chemistry and Pharmacy, University of Southern Denmark, Odense M, 5230, Denmark, Center for Oxygen Microscopy and Imaging, Department of Chemistry, Aarhus University, Langelandsgade 140, Aarhus, 8000, Denmark, Department of Molecular Biology, Aarhus University, Gustav Wieds vej 10, Aarhus, 8000, Denmark, and Center for Bioinformatics and Institute of Physical Chemistry, University of Hamburg, Bundesstraße 43, 20146 Hamburg, Germany

E-mail: kongsted@sdu.dk; progilby@chem.au.dk; ove@chem.au.dk

[*]To whom correspondence should be addressed
[†]University of Southern Denmark
[‡]Aarhus University
[¶]Aarhus University
[§]University of Hamburg

Electronic Supplementary Material (ESI) for Physical Chemistry Chemical Physics
This journal is © The Owner Societies 2014

Computational Details

Homology Modeling and Protein Setup

The miniSOG homology model was generated using SWISS-MODEL.[1] To initiate the modeling, the workspace was given the 106 amino acid primary structure of miniSOG. Based on this, the LOV2 domain from Oat (*Avena sativa*),[2] which is 86.8% sequence identical to miniSOG, was identified as a suitable modeling template. The resultant miniSOG homology modeling structure is characterized by a QMEAN4 score of 0.871 indicating good overall model quality.[3] Furthermore, it was found that all residues interacting with FMN are completely conserved between the model and the template, thus adding further confidence to the quality of the modeled micro environment of FMN in miniSOG.

The resultant protein structure was then prepared for subsequent MD simulations using the Protein Preparation Wizard[4] in the graphical interface Maestro[5] implemented in the Schrödinger Suite. Hydrogen atoms were added to the structure in accordance with the pH value in the experiments (pH 7). Hence, all Lys and Arg residues were positively charged while all Asp and Glu were negatively charged. Protonation states and tautomeric forms of the imidazole ring of His85 were determined using the Protein Assignment and confirmed by visual inspection. On this basis, His85 was assumed to be positively charged. In addition, the flip states of the Gln and Asn residues were examined, and this resulted in a flip of the side chain amide of Gln50.

MD simulations

Following Ref. 6, the generalized Amber force field[7] (GAFF) parameters was employed for the representation of FMN. . In the chromophore/protein simulation, the Amber99SB[8,9] force field was applied for the miniSOG protein. In accordance with the use of GAFF, the atomic partial charges were generated using the restrained electrostatic potential (RESP) approach[10] based on the electrostatic potential obtained at the HF/6-31G* level using Gaussian09.[11] The adopted atom types and charges for FMN are provided in Table S1. The chromophore was solvated in a TIP3P[12]

cubic box extending 12.0 Å from the solute, while a truncated octahedral solvent box of 10.0 Å was used to solvate the protein-cofactor system. Sodium ions were added to maintain charge neutrality of the system. The setup for the MD simulation and the production run were conducted using the modules in the Amber package.[13] The Shake algorithm[14] was employed to remove bond stretching freedom of the solvent molecules. The integration of the equations of motion was performed in time-steps of 0.5 fs, and the temperature was maintained at 300 K using the Berendsen thermostat with a time constant of 1.0 ps. Long-range electrostatic interactions were treated by the Particle Mesh Ewald (PME) method.[15,16] A non-bonded cutoff radius of 10.0 Å was employed and the non-bonded pairlist was updated whenever an atom had moved a distance exceeding 1.0 Å. Prior to the production run, a two-step equilibration procedure was carried out, initiated from the homology model; first, a 50 ps density equilibration in the NPT ensemble followed by a 200 ps simulation in the NVT ensemble. Subsequent to the equilibration phase, a production run of 1 ns was performed in the NVT ensemble and frames were recorded every 20 ps. The structurally confined chromophore in the protein is adequately sampled during this simulation time, as has been confirmed on the basis of a longer simulation (10 ns). The resultant two sets of each 50 molecular configurations were then prepared for the subsequent PE-DFT property calculations; first, the chromophore was reimaged into the center of the simulation box followed by truncation of the solvation box by a distance-based cutoff of 11.0 Å from the FMN molecule in the case of the pure solute-solvent system while a cutoff of 10.0 Å was used for the composite chromophore-protein system. The large cut-off value for the protein-cofactor system was applied to ensure sufficient hydration of the negatively charged ribityl-5'-phosphate tail of FMN which due to the length of the chromophore compared to the protein cavity, is exposed to the bulk solvent.

Geometry optimization

To obtain reliable one- and two-photon optical properties of FMN, it is essential to have reasonable structure, and as previously reported,[17–19] structures generated by classical force fields are often not accurate enough to be used directly in electronic structure calculations. Therefore, each

This journal is © The Owner Societies 2014

Table S1: GAFF atom types and RESP charges (HF/6-31G*) adopted for the FMN chromophore in the two MD simulations. The atom number refers to the labeling in Figure S1.

Atom no.	Type	Charge	Atom no.	Type	Charge
1	nb	-0.751	26	c3	0.293
2	c	0.997	27	os	-0.649
3	o	-0.662	28	p5	1.466
4	n	-0.801	29	o	-0.984
5	c	0.775	30	o	-0.984
6	o	-0.638	31	o	-0.984
7	cd	0.105	32	hn	0.392
8	nb	-0.497	33	ha	0.218
9	ca	0.511	34-36	hc	0.067
10	ca	-0.426	37-39	hc	0.102
11	ca	0.086	40	ha	0.297
12	c3	-0.210	41-42	h1	0.160
13	ca	0.184	43	h1	0.028
14	c3	-0.321	44	ho	0.418
15	ca	-0.360	45	h1	0.132
16	ca	-0.079	46	ho	0.514
17	na	0.095	47	h1	-0.013
18	cd	0.413	48	ho	0.459
19	c3	-0.339	49-50	h1	-0.011
20	c3	0.418			
21	oh	-0.707			
22	c3	0.213			
23	oh	-0.823			
24	c3	0.054			
25	oh	-0.644			

configuration was QM/MM geometry-optimized prior to the QM calculations. These optimizations were conducted using the B3LYP[20–23] exchange correlation (xc) functional in conjunction with the 6-31+G*[24–26] basis set to describe FMN. The potential of charge-penetration into the environment, which is particularly critical in this case due to the high electron density in the tail of the chromophore and a positively charged nearby environment combined with the missing account of exchange-repulsion in the embedding potential, has previously been remedied by defining the phosphate tail as part of the MM region.[27–29] However, this produces an undesired QM/MM boundary traversing a covalent bond. To circumvent this, we used an alternative protocol, where

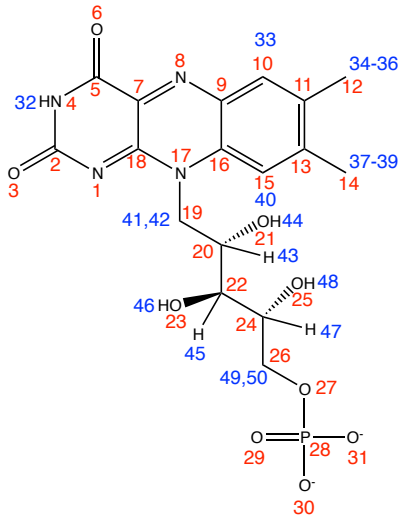

Figure S1: Atom labeling used in Table S1 to identify GAFF atom types. Labels for heavy atoms are red, while those for hydrogen atoms are blue.

a sodium ion located next to the phosphate group of FMN was included in the QM portion, giving a total charge of the QM region of -1. The MM region was represented by the OPLS2005 all-atom force field[30] and the positions of the atoms included in this region (protein, solvent and remaining ions) were kept fixed at the geometry extracted from the MD simulation. The QM/MM optimizations were performed using Qsite 5.8[31–33] in the Schrödinger Suite.

As a further comparison we also report calculations on gas phase lumiflavin (LF). The geometry optimization of LF in the gaseous phase has been performed in Gaussian09[11] using the B3LYP xc-functional and the 6-31+G* basis set (cc-pVTZ for the basis set analysis) to be consistent with the level of theory applied in the QM/MM geometry optimizations of FMN in the two environments.

Electronic Structure Calculations

The vertical excitation energies, one-photon oscillator strengths and two-photon absorption transition probabilities of FMN and isolated LF were evaluated from an analysis of the poles and residues of the linear and quadratic response function within the framework of polarizable embedding time-dependent DFT (PE-TDDFT[34]) as implemented in a development version of DALTON 2011.[35] As shown in Table S2, a preliminary test on microhydrated LF (5 water molecules) indicated that the

effects of hydrogen bonding on the optical properties of LF is well-captured at the PE level, and thus, a QM region containing only the chromophore is sufficient in the present case. The dipole operator in the length-gauge was used for the calculation of the transition moments. Of interest to this study are the two lowest $\pi - \pi^*$ and $n - \pi^*$ transitions of FMN located in the low-energy region of the visible spectrum.

Table S2: The CAM-B3LYP/cc-pVDZ+ one-photon excitation energies (eV) and oscillator strengths of the two lowest $\pi - \pi^*$ and $n - \pi^*$ transitions of LF and microsolvated LF, describing the water molecules either at the QM level or using PE. The geometry of LF is identical in all three cases and is derived from a full QM geometry optimization of the microsolvated LF at the B3LYP/6-311++G level of theory.**

	LF		LF+QM waters		LF+PE waters	
Transition[a]	E_{ex}	f	E_{ex}	f	E_{ex}	f
$\pi_H - \pi_L^*$	2.92	0.262	2.80	0.232	2.82	0.243
$n_N - \pi_L^*$	3.52	0.001	3.59	0.001	3.63	0.001
$\pi_{H-1} - \pi_L^*$	4.00	0.154	3.79	0.199	3.84	0.190
$n_O - \pi_L^*$	3.63	-	4.09	-	4.03	-

[a] H=HOMO, L=LUMO, N=Nitrogen, O=Oxygen.

The two-photon transition probabilities were determined assuming resonant absorption of two identical photons and linear polarization of the light. Following Ref. 36, all properties were computed using the CAM-B3LYP[37] xc-functional and the cc-pVDZ+ basis set derived from Dunning's correlation consistent double-ζ basis set by introducing diffuse s- and p-functions from the augmented counterpart[38,39] on all heavy atoms. The cc-pVDZ basis set was used for sodium. In a preceding basis set analysis effectuated on bare LF (B3LYP/cc-pVTZ geometry), cf. Table S3, the cc-pVDZ+ basis set was shown to provide converged one- and two-photon properties of the four considered transitions by comparison to the corresponding aug-cc-pVDZ and aug-cc-pVTZ results.

Note that the $n - \pi^*$ transitions of LF in the gaseous phase are subject to some controversy since their ordering and character (lonepair orbitals on nitrogen or oxygen) change among methods. The description of the $n - \pi^*$ transitions obtained in this work using CAM-B3LYP is in agreement with

Table S3: Excitation energies E_{ex} (eV), one-photon oscillator strengths f and two-photon transition probabilities δ^{TPA} (a.u.) of the two lowest $\pi-\pi^*$ and $n-\pi^*$ transitions[a] of LF in vacuum computed at the CAM-B3LYP/cc-pVDZ+ level of theory.

Transition[a]	Basis set	E_{ex}	f	δ^{TPA}
$\pi_H-\pi_L^*$	cc-pVDZ+	3.35	0.310	129
	aug-cc-pVDZ	3.33	0.302	126
	aug-cc-pVTZ	3.33	0.303	129
$n_N-\pi_L^*$	cc-pVDZ+	3.61	0.001	1.1
	aug-cc-pVDZ	3.61	0.001	0.9
	aug-cc-pVTZ	3.60	0.001	0.9
$n_O-\pi_L^*$	cc-pVDZ+	3.98	-	0.1
	aug-cc-pVDZ	3.98	-	0.1
	aug-cc-pVTZ	3.98	-	0.1
$\pi_{H-1}-\pi_L^*$	cc-pVDZ+	4.28	0.137	217
	aug-cc-pVDZ	4.27	0.132	227
	aug-cc-pVTZ	4.25	0.134	228

[a] H=HOMO, L=LUMO, N=Nitrogen, O=Oxygen.

previous SAC-CI[40] and CASPT2[41] results, whereas the states are flipped and an additional state is found using DFT(BHLYP)/MRCI[42] and TDDFT/B3LYP.[43–45] However, since a consistent picture across methods is found when going to the condensed phase,[40,46] we shall not be concerned further with this discrepancy restricted to the isolated case.

To validate the use of the PE-TDDFT calculations, PE resolution of identity approximate second order coupled cluster (PERI-CC2[47,48]) calculations were carried out using a development version of TURBOMOLE V6.4.[49] Due to the large size of FMN, we can only benchmark TDDFT one-photon calculations against PERI-CC2, however, CC2 has in fact been shown to give quite good results relative to results including effects of triples excitations for smaller molecules.[50] We employed the cc-pVDZ+ basis in combination with the corresponding auxiliary basis set[51,52] to treat the four-index electron repulsion integrals in the RI approximation.[53]

The PE model was adopted to evaluate the influence of the surrounding environment on the chromophore properties. The solvent molecules and the protein were represented by a classical

embedding potential, while, as in the QM/MM geometry optimizations, the FMN chromophore and a nearby sodium ion were treated quantum-mechanically. The absorption spectra are hardly modified by the sodium ion and its inclusion in the QM region only serves to set up a repulsive potential, as described above. The permanent charge distribution of the environment was described by assigning a point charge to each atom, and the induced potential was modeled using distributed isotropic electronic dipole-dipole polarizabilities.

The generation of the embedding potential of each configuration was handled using the PEAS program,[54] and the molecular fractionation with conjugated caps (MFCC) fragmentation approach[55] was used to decompose the protein into capped amino acids. The atomic point charges were computed for the resultant protein fragments and ions located in the classical region using the RESP procedure at the B3LYP/6-31+G* level, while the atomic isotropic dipole-dipole polarizabilities were determined at the same level of theory (the ANO-S basis set was used for the sodium ions) using the localized properties (LoProp) approach[56] implemented in Molcas.[57] The basis set was recontracted to an atomic natural orbital (ANO) type basis set, as required by the localization procedure. The insufficient description of the hydrogen atoms offered by the 6-31+G* basis set along with its relatively high abundance in water leads to a significantly underestimated molecular polarizability for water.[58] Therefore, to model aqueous solution, we used a different potential to describe the water molecules - the Ahlström potential[59] - consisting of atomic point charges and a molecular isotropic polarizability located at the oxygen atom. To avoid overpolarization of the induced dipoles within the classical region, the exponential damping scheme by Thole[60] was employed.

Figure S2 presents the convergence of the resulting excitation energies of the two lowest $\pi - \pi^*$ transitions of miniSOG as a function of the simulation time. As is evident from this figure, including 50 snapshots in the averaging leads to converged results. In fact it would be possible to obtain converged results using a fewer number of snapshots but this would, on the other hand, lead to a higher error in the mean values.

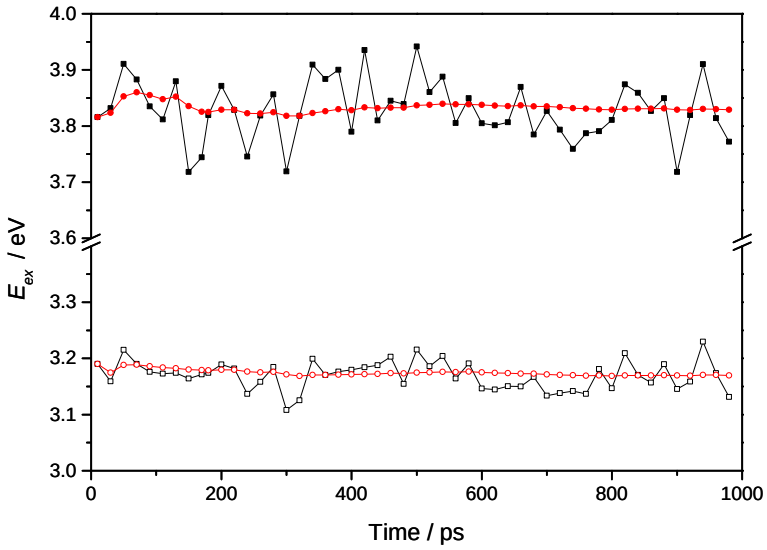

Figure S2: Excitation energies of the two lowest $\pi - \pi^*$ transitions (squares) of miniSOG and the associated running averages (circles) along the MD trajectory after QM/MM geometry optimization of each configuration (see text).

Generation of Simulated Spectra

The simulated one-photon spectra were obtained as the spectral average over the spectrum of each snapshot n, where each transition i was convoluted with a Gaussian line shape function

$$I_n^{\mathrm{OPA}}(\omega) = \frac{1}{\sigma\sqrt{2\pi}} \sum_i f_{n_i} \exp\left(-\frac{1}{2}\left(\frac{\omega - \omega_{n_i}}{\sigma}\right)^2\right), \tag{1}$$

to account for natural line broadening. Here, ω_i is the excitation energy of the ith transition, while the σ-value is related to the full width at half maximum (FWHM) as $\Gamma = 2\sqrt{2\ln 2}\sigma$. Γ was set to 0.35 eV for all one- and two-photon transitions.

From a microscopic point of view, the central molecular quantity describing the two-photon absorption of a molecule in gas-phase is the two-photon transition matrix element. The two-photon transition matrix element (a.u.), corresponding to resonant absorption of two monochromatic photons, is related to the single residue of the quadratic response function, when evaluating the latter

at a frequency equal to half of the excitation energy from the ground to the specific excited state

$$S_{\alpha\beta} = \sum_i \left[\frac{\langle 0|\hat{\mu}_\alpha|i\rangle\langle i|\hat{\mu}_\beta|f\rangle}{\omega_i - \omega_f/2} + \frac{\langle 0|\hat{\mu}_\beta|i\rangle\langle i|\hat{\mu}_\alpha|f\rangle}{\omega_i - \omega_f/2} \right], \tag{2}$$

in which $\alpha, \beta = \{x, y, z\}$ and $\hat{\mu}_\alpha$ is a component of the electric dipole operator while ω_i and ω_f are the excitation energies from the ground, $|0\rangle$, to intermediate, $|i\rangle$, and final states $|f\rangle$, respectively. The summation runs over all excited states and the ground state. When considering linearly polarized light, the orientationally averaged two-photon absorption transition probability can be written as[61,62]

$$\delta^{\mathrm{TPA}} = \frac{1}{15} \sum_{\alpha\beta} \left[S_{\alpha\alpha} S^*_{\beta\beta} + 2 S_{\alpha\beta} S^*_{\alpha\beta} \right], \tag{3}$$

where we have used that S is symmetric, as can be inferred from Eq. 2. The conversion of the two-photon absorption transition probabilities (in a.u.) to the physically observable two-photon absorption cross section (in GM) proceeds according to[63]

$$\sigma^{\mathrm{TPA}}(\omega) = \frac{4\pi^3 \alpha a_0^5 \omega^2}{c} g(2\omega) \delta^{\mathrm{TPA}}, \tag{4}$$

where α is the fine structure constant, a_0 is the Bohr radius (cm), c the speed of light (cm s^{-1}), ω is the energy of the incoming photons (a.u.). Here, $g(2\omega)$ is a normalized Gaussian line-shape function

$$g(2\omega) = \frac{2}{\Gamma} \sqrt{\frac{\ln(2)}{\pi}} \exp\left(-4\ln(2) \left(\frac{2\omega - \omega_i}{\Gamma} \right)^2 \right). \tag{5}$$

In analogy to the one-photon case, the two-photon spectra were obtained as the average of the spectral contribution from each snapshot

$$I_n^{\mathrm{TPA}}(\omega) = \sum_i \sigma_{n_i}^{\mathrm{TPA}}(\omega). \tag{6}$$

This journal is © The Owner Societies 2014

Molecular Structure and Conformation

Consistent with previous studies on solvated LF (modeled by a continuum model and/or micro-hydration model),[40,42] we observe a lengthening of the CO and NH bonds with respect to the isolated case. This is expected due to the formation of the hydrogen bonds to water molecules. The hydrogen bonding to the environment is also manifested in a contraction of the bond lengths of the formal C-N single bonds in the ring system by ca. 1.5-2.0 pm, while the formal double bonds are generally lengthened due to the presence of the solvent. The planarity of the flavin ring structure, characterizing isolated LF, is distorted in solvated FMN, as can be seen from a 0.155 Å root-mean-square deviation (RMSD) of the distances of the heavy atoms of the flavin moiety to a plane, defined by a least-square plane fit to the same set of heavy atoms. Excluding the methylene C atom, directly bonded to flavin, in the least-square fit leads to a smaller deviations from planarity, i.e. with RMSD = 0.128 Å, showing that the flexibility of the tail in the solvent distorts the optically active part of FMN.

Inspection of Table S3 shows that the protein environment induces similar, although less serious, structural modifications as in aqueous solution. This can be rationalized on the basis of the local environment of the chromophore inside miniSOG. Within the spatially organized protein matrix, the flavin moiety of FMN is engaged in hydrogen bond formation to the Gln103, Asn72 and Gln44 residues (Figure 1 of the main text), and no charged residues are located in the immediate vicinity of the flavin part. The NH group of FMN competes with the amide side-chain of Asn82 in hydrogen bonding with the carbonyl group of the side-chain amide of Asn72 that rotates so as to alternately optimize its interaction to each of these groups. In fact, these four amino acids are highly conserved in the wild type primary structure of LOV domains from various organisms.[64–66] The above analysis indicates that the hydrogen bonds formed between FMN in water are stronger than the corresponding hydrogen bonds formed between FMN and these key residues. In addition to these hydrogen bonds, the hydroxy groups of the ribityl-5'-phosphate chain participate in hydrogen bonding to the protein scaffold as well as to two biological water molecules that are situated at the phenyl side of the chromophore. During the MD simulation an exchange of one of these water

This journal is © The Owner Societies 2014

molecules and bulk water was observed. The presence of water molecules in this region of the binding pocket is in line with a previous study on the Phot-LOV1 domain from *Chlamydomonas reinhardtii*.[28]

Table S4: Ground state bond distances (Å) of FMN in aqueous solution and inside miniSOG, averaged over sampled configurations, in comparison with those of isolated LF. The atomic labels are depicted in Figure 4A of the main text. Apart from the N3-H bond of FMN in aqueous solution, which has the largest standard deviation of 1.25 pm, fluctuations in bond distances are below 0.5 and 1.0 pm for FMN in miniSOG and water, respectively.

The averaged RMSD (Å) of the distance from the heavy atoms of the flavin moiety to a plane, defined by a least-square plane fit to the same atoms. The structures have been obtained at the B3LYP/6-31+G* level of theory.

	In water	In protein	Isolated LF
N1-C2	1.358	1.366	1.381
C2-N3	1.397	1.405	1.416
N3-C4	1.361	1.370	1.381
C4-C4a	1.480	1.491	1.500
C4a-N5	1.305	1.304	1.299
N5-C5a	1.355	1.361	1.368
C5a-C6	1.413	1.412	1.411
C6-C7	1.378	1.380	1.385
C7-C7c	1.506	1.505	1.510
C7-C8	1.430	1.427	1.425
C8-C8c	1.503	1.505	1.509
C8-C9	1.389	1.388	1.394
C9-C9a	1.403	1.404	1.406
C9a-N10	1.387	1.386	1.388
N10-C10a	1.370	1.373	1.384
C10a-N1	1.320	1.316	1.308
C5a-C9a	1.426	1.422	1.420
C4a-C10a	1.444	1.452	1.463
N10-R	1.480	1.471	1.469
C2-O2	1.235	1.230	1.221
C4-O4	1.229	1.226	1.219
N3-H	1.026	1.025	1.016
RMSD	0.155	0.116	-

References

(1) Arnold, K.; Bordoli, L.; Kopp, J.; Schwede, T. The SWISS-MODEL Workspace: a Web-Based Environment for Protein Structure Homology Modelling. *Bioinformatics* **2006**, *22*, 195–201.

(2) Halavaty, A. S.; Moffat, K. N-and C-terminal Flanking Regions Modulate Light-Induced Signal Transduction in the LOV2 Domain of the Blue Light Sensor Phototropin 1 from *Avena Sativa*. *Biochemistry* **2007**, *46*, 14001–14009.

(3) Benkert, P.; Biasini, M.; Schwede, T. Toward the Estimation of the Absolute Quality of Individual Protein Structure Models. *Bioinformatics* **2011**, *27*, 343–350.

(4) Schrödinger Suite 2011 Protein Preparation Wizard; Epik version 2.2, Schrödinger , LLC, New York , NY, 2011, Impact version 5.7, Schrödinger, LCC, New York, NY, 2011; Prime version 3.0, Schrödinger , LLC, New York, NY, 2011.

(5) Maestro 9.2, Schrödinger, LCC, New York, NY, 2011.

(6) Khrenova, M. G.; Nemukhin, A. V.; Grigorenko, B. L.; Krylov, A. I.; Domratcheva, T. M. Quantum Chemistry Calculations Provide Support to the Mechanism of the Light-Induced Structural Changes in the Flavin-Binding Photoreceptor Proteins. *J. Chem. Theory Comput.* **2010**, *6*, 2293–2302.

(7) Wang, J.; Wolf, R. M.; Caldwell, J. W.; Kollman, P. A.; Case, D. A. Development and Testing of a General Amber Force Field. *J. Comput. Chem.* **2004**, *25*, 1157–1174.

(8) Hornak, V.; Abel, R.; Okur, A.; Strockbine, B.; Roitberg, A.; Simmerling, C. Comparison of Multiple Amber Force Fields and Development of Improved Protein Backbone Parameters. *Proteins: Struct., Funct., and Bioinf.* **2006**, *65*, 712–725.

(9) Cornell, W. D.; Cieplak, P.; Bayly, C. I.; Gould, I. R.; Merz, K. M.; Ferguson, D. M.; Spellmeyer, D. C.; Fox, T.; Caldwell, J. W.; Kollman, P. A. A Second Generation Force Field for the Simulation of Proteins, Nucleic Acids, and Organic Molecules. *J. Am. Chem. Soc.* **1995**, *117*, 5179–5197.

(10) Bayly, C. I.; Cieplak, P.; Cornell, W. D.; Kollman, P. A. A Well-Behaved Electrostatic Potential Based Method Using Charge Restraints for Deriving Atomic Charges: the RESP model. *J. Phys. Chem.* **1993**, *97*, 10269–10280.

(11) Frisch, M. J. et al. Gaussian 09 Revision A.02. Gaussian Inc. Wallingford CT 2009.

(12) Jorgensen, W. L. Quantum and Statistical Mechanical Studies of Liquids. 10. Transferable Intermolecular Potential Functions for Water, Alcohols, and Ethers. Application to Liquid Water. *J. Am. Chem. Soc.* **1981**, *103*, 335–340.

(13) Case, D. A. et al. AMBER 9. 2006; University of California, San Francisco.

(14) Ryckaert, J. P.; Ciccotti, G.; Berendsen, H. J. C. Numerical Integration of the Cartesian Equations of Motion of a System with Constraints: Molecular Dynamics of *N*-alkanes. *J. Comput. Phys.* **1977**, *23*, 327–341.

(15) Essmann, U.; Perera, L.; Berkowitz, M. L.; Darden, T.; Lee, H.; Pedersen, L. G. A Smooth Particle Mesh Ewald Method. *J. Chem. Phys.* **1995**, *103*, 8577–8593.

(16) Darden, T.; York, D.; Pedersen, L. Particle Mesh Ewald: An N-Log (N) Method for Ewald Sums in Large Systems. *J. Chem. Phys.* **1993**, *98*, 10089–10092.

(17) Hsiao, Y.-W.; Sanchez-Garcia, E.; Doerr, M.; Thiel, W. Quantum Refinement of Protein Structures: Implementation and Application to the Red Fluorescent Protein DsRed.M1. *J. Phys. Chem. B* **2010**, *114*, 15413–15423.

(18) Beerepoot, M.; Steindal, A. H.; Kongsted, J.; Brandsdal, B. O.; Frediani, L.; Ruud, K.; Olsen, J. M. H. A Polarizable Embedding DFT Study of One-Photon Absorption in Fluorescent Proteins. *Phys. Chem. Chem. Phys.* **2013**, *15*, 4735–4743.

(19) Eriksen, J. J.; Olsen, J. M. H.; Aidas, K.; Ågren, H.; Mikkelsen, K. V.; Kongsted, J. Computational Protocols for Prediction of Solute NMR Relative Chemical Shifts. A case study of L-Tryptophan in Aqueous Solution. *J. Comp. Chem.* **2011**, *32*, 2853–2864.

(20) Becke, A. D. Density-Functional Thermochemistry. III. The Role of Exact Exchange. *J. Chem. Phys.* **1993**, *98*, 5648.

(21) Vosko, S. H.; Wilk, L.; Nusair, M. Accurate Spin-Dependent Electron Liquid Correlation Energies for Local Spin Density Calculations: a Critical Analysis. *Can. J. Phys.* **1980**, *58*, 1200–1211.

(22) Stephens, P. J.; Devlin, F. J.; Chabalowski, C. F.; Frisch, M. J. Ab Initio Calculation of Vibrational Absorption and Circular Dichroism Spectra using Density Functional Force Fields. *J. Phys. Chem.* **1994**, *98*, 11623–11627.

(23) Lee, C.; W., Y.; Parr, R. G. Development of the Colle-Salvetti Correlation-Energy Formula into a Functional of the Electron Density. *Phys. Rev. B.* **1988**, *37*, 785–789.

(24) Hehre, W. J.; Ditchfield, R.; Pople, J. A. Self Consistent Molecular Orbital Methods. XII. Further Extensions of Gaussian–Type Basis Sets for Use in Molecular Orbital Studies of Organic Molecules. *J. Chem. Phys.* **1972**, *56*, 2257–2261.

(25) Hariharan, P. C.; Pople, J. A. The Influence of Polarization Functions on Molecular Orbital Hydrogenation Energies. *Theor. Chim. Acta* **1973**, *28*, 213–222.

(26) Clark, T.; Chandrasekhar, J.; Spitznagel, G. W.; Schleyer, P. V. R. Efficient Diffuse Function-Augmented Basis Sets for Anion Calculations. III. The 3-21+G Basis Set for First-Row Elements, Li-F. *J. Comput. Chem.* **1983**, *4*, 294–301.

(27) Salzmann, S.; Silva-Junior, M. R.; Thiel, W.; Marian, C. M. Influence of the LOV Domain on Low-Lying Excited States of Flavin: A Combined Quantum-Mechanics/Molecular-Mechanics Investigation. *J. Phys. Chem. B* **2009**, *113*, 15610–15618.

(28) Dittrich, M.; Freddolino, P. L.; Schulten, K. When Light Falls in LOV: a Quantum Mechanical/Molecular Mechanical Study of Photoexcitation in Phot-LOV1 of *Chlamydomonas Reinhardtii*. *J. Phys. Chem. B* **2005**, *109*, 13006–13013.

(29) Domratcheva, T.; Fedorov, R.; Schlichting, I. Analysis of the Primary Photocycle Reactions Occurring in the Light, Oxygen, and Voltage Blue-Light Receptor by Multiconfigurational Quantum-Chemical Methods. *J. Chem. Theory Comput.* **2006**, *2*, 1565–1574.

(30) Kaminski, G. A.; Friesner, R. A.; Tirado-Rives, J.; Jorgensen, W. L. Evaluation and Reparametrization of the OPLS-AA Force Field for Proteins via Comparison with Accurate Quantum Chemical Calculations on Peptides. *J. Phys. Chem. B* **2001**, *105*, 6474–6487.

(31) QSite, version 5.8, Schrödinger, LLC, New York, NY. 2012.

(32) Murphy, R. B.; Philipp, D. M.; Friesner, R. A. A Mixed Quantum Mechanics/Molecular Mechanics (QM/MM) Method for Large-Scale Modeling of Chemistry in Protein Environments. *J. Comput. Chem.* **2000**, *21*, 1442–1457.

(33) Philipp, D. M.; Friesner, R. A. Mixed Ab Initio QM/MM Modeling using Frozen Orbitals and Tests with Alanine Dipeptide and Tetrapeptide. *J. Comput. Chem.* **1999**, *20*, 1468–1494.

(34) Olsen, J. M.; Aidas, K.; Kongsted, J. Excited States in Solution through Polarizable Embedding. *J. Chem. Theory Comput.* **2010**, *6*, 3721–3720.

(35) *DALTON, a molecular electronic structure program, Release Dalton2011 (2011), see http://daltonprogram.org/*.

(36) Götze, J. P.; Greco, C.; Mitrić, R.; Bonačić-Kouteckỳ, V.; Saalfrank, P. BLUF Hydrogen Network Dynamics and UV/Vis Spectra: A Combined Molecular Dynamics and Quantum Chemical Study. *J. Comp. Chem.* **2012**, *33*, 2233–2242.

(37) Yanai, T.; Tew, D. P.; Handy, N. C. A New Hybrid Exchange–Correlation Functional using the Coulomb-Attenuating Method (CAM-B3LYP). *Chem. Phys. Lett.* **2004**, *393*, 51–57.

(38) Dunning, T. H. Gaussian Basis Sets for use in Correlated Molecular Calculations. I. The Atoms Boron through Neon and Hydrogen. *J. Chem. Phys.* **1989**, *90*, 1007–1023.

(39) Kendall, R. A.; Dunning Jr, T. H.; Harrison, R. J. Electron Affinities of the First-Row Atoms Revisited. Systematic Basis Sets and Wave Functions. *J. Chem. Phys* **1992**, *96*, 6796–6806.

(40) Hasegawa, J.; Bureekaew, S.; Nakatsuji, H. SAC-CI Theoretical Study on the Excited States of Lumiflavin: Structure, Excitation Spectrum, and Solvation Effect. *J. Photochem. Photobiol., A: Chemistry* **2007**, *189*, 205–210.

(41) Climent, T.; González-Luque, R.; Merchán, M.; Serrano-Andrés, L. Theoretical Insight into the Spectroscopy and Photochemistry of Isoalloxazine, the Flavin Core Ring. *J. Phys. Chem. A* **2006**, *110*, 13584–13590.

(42) Salzmann, S.; Tatchen, J.; Marian, C. M. The Photophysics of Flavins: What Makes the Difference Between Gas Phase and Aqueous Solution? *J. Photochem. Photobiol., A: Chemistry* **2008**, *198*, 221–231.

(43) Zenichowski, K.; Gothe, M.; Saalfrank, P. Exciting Flavins: Absorption Spectra and Spin–Orbit Coupling in Light–Oxygen–Voltage (LOV) Domains. *J. Photochem. Photobiol., A: Chemistry* **2007**, *190*, 290–300.

(44) Neiss, C.; Saalfrank, P.; Parac, M.; Grimme, S. Quantum Chemical Calculation of Excited States of Flavin-Related Molecules. *J. Phys. Chem. A* **2003**, *107*, 140–147.

(45) Sikorska, E.; Khmelinskii, I. V.; Prukala, W.; Williams, S. L.; Patel, M.; Worrall, D. R.; Bourdelande, J. L.; Koput, J.; Sikorski, M. Spectroscopy and Photophysics of Lumiflavins and Lumichromes. *J. Phys. Chem. A* **2004**, *108*, 1501–1508.

(46) Salzmann, S.; Martinez-Junza, V.; Zorn, B.; Braslavsky, S. E.; Mansurova, M.; Marian, C. M.; Gärtner, W. Photophysical Properties of Structurally and Electronically Modified Flavin Derivatives determined by Spectroscopy and Theoretical Calculations. *J. Phys. Chem. A* **2009**, *113*, 9365–9375.

(47) Sneskov, K.; Schwabe, T.; Kongsted, J.; Christiansen, O. The Polarizable Embedding Coupled Cluster Method. *J. Chem. Phys.* **2011**, *134*, 104108.

(48) Schwabe, T.; Sneskov, K.; Olsen, J. M.; Kongsted, J.; Christiansen, O.; Hättig, C. PERI-CC2: A Polarizable Embedded RI-CC2 Method. *J. Chem. Theory Comput.* **2012**, *8*, 3274–3283.

(49) TURBOMOLE V6.4 2012, a development of University of Karlsruhe and Forschungszentrum Karlsruhe GmbH, 1989-2007, TURBOMOLE GmbH, since 2007; available from `http://www.turbomole.com`.

(50) Schreiber, M.; Silva-Junior, M. R.; Sauer, S. P. A.; Thiel, W. Benchmarks for Electronically Excited States: CASPT2, CC2, CCSD, and CC3. *J. Chem. Phys.* **2008**, *128*, 134110–134134.

(51) Weigend, F.; Köhn, A.; Hättig, C. Efficient Use of the Correlation Consistent Basis Sets in Resolution of the Identity MP2 Calculations. *J. Chem. Phys.* **2002**, *116*, 3175–3183.

(52) Hättig, C. Optimization of Auxiliary Basis Sets for RI-MP2 and RI-CC2 Calculations: CoreâĂŞValence and Quintuple-Îű Basis Sets for H to Ar and QZVPP Basis Sets for Li to Kr. *Phys. Chem. Chem. Phys.* **2005**, *7*, 59–66.

(53) Hättig, C.; Weigend, F. CC2 Excitation Energy Calculations on Large Molecules using the Resolution of the Identity Approximation. *J. Chem. Phys.* **2000**, *113*, 5154–5161.

(54) Olsen, J. M. H. Development of Quantum Chemical Methods towards Rationalization and Optimal Design of Photoactive Proteins. Ph.D. thesis, University of Southern Denmark, Odense, Denmark, 2012; DOI: 10.6084/m9.figshare.156851.

(55) Zhang, D. W.; Zhang, J. Z. H. Molecular Fractionation with Conjugate Caps for Full Quantum Mechanical Calculation of Protein–Molecule Interaction Energy. *J. Chem. Phys.* **2003**, *119*, 3599.

(56) Gagliardi, L.; Lindh, R.; Karlström, G. Local Properties of Quantum Chemical Systems: The LoProp Approach. *J. Chem. Phys.* **2004**, *121*, 4494.

(57) Aquilante, F.; De Vico, L.; Ferré, N.; Ghigo, G.; Malmqvist, P. Å.; Neogrády, P.; Pedersen, T. B.; Pitoňák, M.; Reiher, M.; Roos, B. O.; Serrano-Andrés, L.; Urban, M.; Veryazov, V.; Lindh, R. MOLCAS 7: The Next Generation. *J. Comp. Chem.* **2010**, *31*, 224.

(58) Aidas, K.; Olsen, J. M. H.; Kongsted, J.; Ågren, H. Photoabsorption of Acridine Yellow and Proflavin Bound to Human Serum Albumin Studied by Means of Quantum Mechanics/Molecular Dynamics. *J. Phys. Chem. B* **2013**, *117*, 2069–2080.

(59) Ahlström, P.; Wallqvist, A.; Engström, S.; Jönsson, B. A Molecular Dynamics Study of Polarizable Water. *Mol. Phys.* **1989**, *68*, 563–581.

(60) Van Duijnen, P. T.; Swart, M. Molecular and Atomic Polarizabilities: Thole's Model Revisited. *J. Phys. Chem. A* **1998**, *102*, 2399–2407.

(61) Monson, P. R.; McClain, W. M. Polarization Dependence of the Two-Photon Absorption of Tumbling Molecules with Application to Liquid 1-Chloronaphthalene and Benzene. *J. Chem. Phys.* **1970**, *53*, 29.

(62) McClain, W. M., Excited State Symmetry Assignment Through Polarized Two-Photon Absorption Studies of Fluids. *J. Chem. Phys.* **1971**, *55*, 2789–2796.

(63) Frediani, L. and Rinkevicius, Z. and Ågren, H., Two-Photon Absorption in Solution by Means of Time-Dependent Density-Functional Theory and the Polarizable Continuum Model. *J. Chem. Phys.* **2005**, *122*, 244104–244115.

(64) Losi, A. Flavin-Based Blue-Light Photosensors: A Photobiophysics Update. *Photochem. Photobiol.* **2007**, *83*, 1283–1300.

(65) Möglich, A.; Moffat, K. Structural Basis for Light-Dependent Signaling in the Dimeric LOV Domain of the Photosensor YtvA. *J. Mol. Biology* **2007**, *373*, 112–126.

(66) Nakasako, M.; Zikihara, K.; Matsuoka, D.; Katsura, H.; Tokutomi, S. Structural Basis of the LOV1 Dimerization of *Arabidopsis* Phototropins 1 and 2. *J. Mol. Biol.* **2008**, *381*, 718–733.

Table S5: One-photon excitation energies E_{ex} (eV) and one-photon oscillator strengths f of the two lowest $\pi-\pi^*$ and $n-\pi^*$ transitions of FMN for three representative configurations in miniSOG and aqueous solution, respectively, computed at the PE-CAM-B3LYP/cc-pVDZ+ and PERI-CC2/cc-pVDZ+ levels of theory, along with the corresponding differences (Δ).

		In protein						In water					
		CAM-B3LYP		PERI-CC2		Δ		CAM-B3LYP		PERI-CC2		Δ	
Transition[a]	Conf	E_{ex}	f	E_{ex}	f	E_{ex}	f	E_{ex}	f	E_{ex}	f	E_{ex}	f
$\pi_H-\pi_L^*$	1	3.19	0.37	2.88	0.33	0.31	0.04	3.26	0.34	2.95	0.31	0.31	0.03
	2	3.15	0.35	2.82	0.31	0.33	0.04	3.14	0.30	2.82	0.28	0.32	0.02
	3	3.15	0.34	2.82	0.31	0.33	0.03	3.15	0.28	2.83	0.26	0.32	0.02
$n_N-\pi_L^*$	1	3.81	0.03	3.70	0.04	0.11	-0.01	3.83	0.07	3.71	0.04	0.12	0.03
	2	3.76	0.05	3.61	0.01	0.15	0.04	3.72	0.03	3.58	0.00	0.14	0.03
	3	3.71	0.02	3.56	0.00	0.15	0.02	3.74	0.04	3.56	0.05	0.18	-0.01
$\pi_{H-1}-\pi_L^*$	1	3.87	0.23	3.74	0.25	0.13	-0.02	3.75	0.20	3.63	0.26	0.12	-0.06
	2	3.80	0.22	3.67	0.29	0.13	-0.07	3.79	0.25	3.66	0.28	0.13	-0.03
	3	3.81	0.25	3.68	0.28	0.13	-0.03	3.64	0.27	3.51	0.25	0.13	0.02
$n_O-\pi_L^*$	1	4.40	-	4.01	-	0.39	-	4.34	-	4.00	-	0.34	-
	2	4.45	-	4.09	-	0.36	-	4.53	-	4.20	-	0.33	-
	3	4.38	-	4.03	-	0.35	-	4.39	-	4.07	-	0.32	-

[a] *H*=HOMO, *L*=LUMO, *N*=Nitrogen, *O*=Oxygen.

Electronic Supplementary Material (ESI) for Physical Chemistry Chemical Physics
This journal is © The Owner Societies 2014